Damage evolution behavior and damage constitutive model of selective-laser-melted Ti6Al4V alloy under different heat treatment temperatures

Xiaodong Li[1] , Lei li[1], Li Zhang[1], Zhankun Sun[1], Dexin Mao[1]

[1]Inner Mongolia University of Technology. Hohhot, Inner Mongolia, China.
e-mail: 1774837317@qq.com, leillt@163.com, lizhang20031018@163.com, sunzk_cailiao@163.com, 2582887978@qq.com

ABSTRACT

To study the damage evolution behavior and damage constitutive model of selective-laser-melted (SLMed) Ti6Al4V alloy under different heat treatment temperatures, tensile tests were conducted. The effect of heat treatment temperature on microstructure and mechanical properties of SLMed Ti6Al4V alloy is discussed. Elastic modulus was selected to characterize damage, and the damage evolution law of SLMed Ti6Al4V alloy was quantitatively analyzed, establishing the damage evolution equation. Based on the theory of continuous damage mechanics, the Ramberg-Osgood model was introduced to establish the damage constitutive model of SLMed Ti6Al4V alloy under different heat treatment temperatures. The results show that with increasing heat treatment temperature, the acicular α′ phase in the microstructure of SLMed Ti6Al4V alloy is gradually transformed into *α + β phase*, the *α phase* is gradually coarsened, the volume fraction of *β phase* gradually increased. The microhardness and tensile strength of the SLMed Ti6Al4V alloy decreased from 376.44 HV and 1171.5 MPa to 317.31 HV and 790.9 MPa, while elongation increased from 6.6% to 13.6% and then decreased to 11.1%. The critical strain in the as-deposited sample is 0.009, entering the rapid damage accumulation stage first, whereas heat-treated samples lag significantly. The error between model and experimental results is within 7%.

Keywords: Heat treatment; Selective-laser-melted Ti6Al4V alloy; Damage evolution; Damage constitutive model.

1. INTRODUCTION

Ti6Al4V alloy is a medium strength α + β type titanium alloy containing 6% *α phase* stable element Al and 4% *β phase* stable element V. It has advantages of low mass and high strength, good high-temperature strength, corrosion resistance and biocompatibility, and is widely used in petrochemical, aerospace and biomedical fields [1–4]. However, the Ti6Al4V alloy has problems of difficult cutting, low machining efficiency, and long machining cycle in traditional manufacturing processes, which in turn affects the dimensional accuracy and surface roughness of parts.

Recently, with technological development, selective laser melting technology has garnered increasing attention. Selective laser melting is a novel additive manufacturing technology characterized by high forming accuracy, short processing cycle, and the ability to directly form complex components [5–7]. This technology offers high design freedom and manufacturing methods for complex shapes, enabling relatively easy machining of complex components, of particular interest in aerospace, biomedical, and other fields [8]. However, anisotropy and residual stresses in components fabricated by this technique limit its use. Heat treatment has received considerable attention from researchers as a relatively low-cost and effective method to reduce anisotropy and residual stresses in selective-laser-melted (SLMed) components [9]. ZHEN *et al.* [10] found that SLMed Ti6Al4V samples had high strength, poor plasticity, and obvious anisotropy. By cyclic spheroidal annealing + solid solution aging treatment of SLMed Ti6Al4V, the plasticity was significantly improved, with elongation reaching 18.3%. The anisotropy in strength was less than 2%, and mechanical properties exceeded those of ordinary forgings. JABER *et al.* [11] found that the strength and ductility of SLMed Ti6Al4V alloys are determined by subsequent heat treatment. After heat treatment at 850°C, the microstructure consisted mainly of 78.71% *α phase* and 21.29% *β phase*. Its elongation increased by 62.5%, tensile strength decreased by 16.4%, and the overall mechanical properties were optimal. JIANQIANG *et al.* [12] observed that the microstructure

of SLMed Ti6Al4V alloy consisted of acicular *α' phase* and incipient *β phase*. After various heat treatments, the tensile and yield strengths slightly decreased, while plasticity significantly improved. LIANG *et al.* [13] conducted heat treatment experiments on SLMed Ti6Al4V samples and found that after heat treatment at 800°C and 850°C, the microstructure of the samples contained platelet *α phase* with the highest content of *β phase*, exhibiting the best ductility and good ultimate tensile stress.

The studies of the aforementioned scholars show heat treatment can effectively improve microstructure and enhance comprehensive mechanical properties of SLMed Ti6Al4V alloys, enabling wider practical engineering applications. However, in practical engineering, material internal damage accumulation severely affects in-service performance. Under loading conditions, internal damage evolves with deformation and eventually leads to sample destruction. Investigating material damage evolution is important for assessing in-service performance. BO *et al.* [14] found that microhardness, elastic modulus, toughness index, and electrical resistivity changes can effectively characterize the plastic damage process of metal materials, showing regularity and evaluating mechanical properties. ALHARBI *et al.* [15] studied the damage mechanism of DP1000 dual phase steel via in-situ tensile testing using scanning electron microscopy, obtaining the microstructure damage evolution law for DP1000 dual phase steel. LEI *et al.* [16] found that using relative shape factors effectively describes microstructure evolution of T2 pure copper and H62 copper alloy under tensile stress. A damage evolution equation based on shape factors more accurately reflects damage and fracture laws of materials. Currently, researchers mainly focus on the damage direction of traditional metal materials, with relatively few studies on the damage evolution law and damage constitutive model of SLMed Ti6Al4V alloy [17–19]. Therefore, it is necessary to systematically study the damage evolution law and damage constitutive model of SLMed Ti6Al4V alloy.

In summary, this article focuses on microstructure and mechanical properties analysis of SLMed Ti6Al4V alloy at different heat treatment temperatures. Elastic modulus of samples at different strain stages during tensile process was measured via nanoindentation. Elastic modulus was used to characterize damage, with normalization factor obtained by normalizing damage factor. Damage evolution of SLMed Ti6Al4V alloy was quantitatively analyzed via normalization factor. The damage factor was incorporated into the Ramberg-Osgood model, and a damage constitutive model was established for SLMed Ti6Al4V alloy at different heat treatment temperatures. This provides a reference for predicting mechanical properties and conducting accurate numerical analysis of SLMed Ti6Al4V alloy.

2. MATERIALS AND METHODS

2.1. Materials and sample preparation

Selective laser melting uses Ti6Al4V alloy powder with a particle size of 13–53 μm, which is gray in color. The chemical composition is shown in Table 1. Samples were prepared using equipment from German company EOS (model EOS M290). To prevent oxidation, preparation was conducted in an argon atmosphere. Using zigzag scanning, the laser power for printing is 340 W, the scanning speed is 1250 mm/s, and the interlayer angle is 67°. The relative density of the sample was determined to be 98.8% using the Archimedes' principle. The details of the sample forming and the sample size are shown in Figure 1.
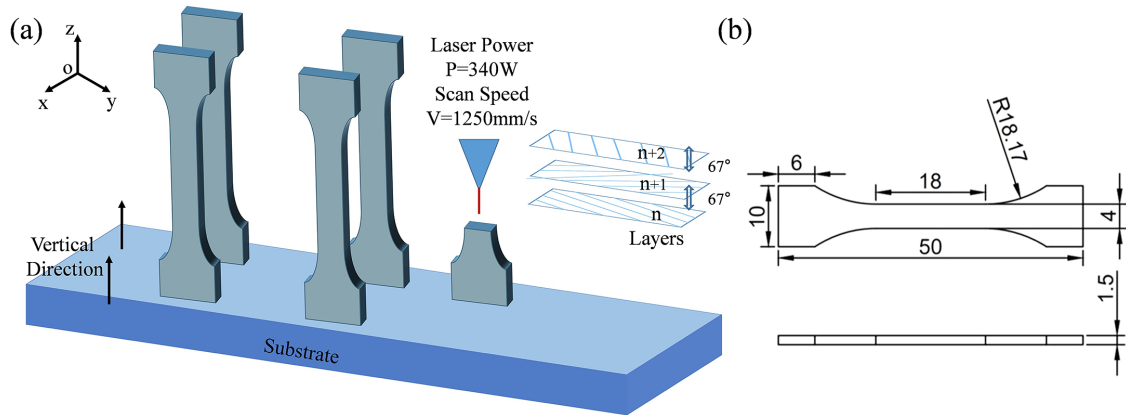
2.2. Heat treatment

For the heat treatment, the tensile samples of the SLMed Ti6Al4V alloy were placed in a pipe furnace (OTF-1200X) at room temperature and heated at a rate of 10°C/min until reaching the required temperatures. To prevent oxidation and nitriding of the sample, an argon atmosphere was maintained during the heat treatment process. The specific heat treatment systems are shown in Table 2.

2.3. Test methods

After polishing the YOZ surface of the sample, use Kroll reagent (HF: HNO3: H2O = 1 ml: 2 ml: 17 ml) for metallographic corrosion. Observe the microstructure of the sample under optical microscopy (OM; LEICA DM6 M) and scanning electron microscopy (SEM; Apreo S Lo Vac). Phase analysis was performed using an X-ray diffractometer (XRD; Bruker D8 Advance) with a scanning range of 20–80° and a scanning speed of 10°/min.

Table 1: Chemical composition of the SLMed Ti6Al4V alloy (wt%).

Al	V	O	Fe	C	N	H	Ti
6.01	4.08	0.097	0.042	0.006	0.005	0.003	bal

Figure 1: (a) schematic of the SLMed Ti6Al4V alloy deposition, (b) dimension of samples (mm).

Table 2: Heat treatment systems of the samples.

| TEMPERATURE	HOLDING TIME	COOLING METHOD
800°C	2 h	Furnace cooling
850°C	2 h	Furnace cooling
900°C	2 h	Furnace cooling
950°C	2 h	Furnace cooling

The Vickers microhardness of the YOZ surface of the samples was obtained using a microhardness tester (HV-1000) with a test force of 1.96 N and holding time of 10 s. A material testing machine (MTS Landmark) was used to perform tensile tests on the samples at a rate of 1 mm/min, and a laser extensometer (MTS Laser Extensometer LX500) was selected for non-contact displacement measurements. The elastic modulus of the YOZ surface of the sample was measured at different strain stages using a nanoindentation instrument (Nano Indenter G200). The nanoindentation test force is 400 mN, the loading rate is 5 mN/s, and the holding time is 10 s.

3. RESULTS AND DISCUSSION

3.1. Microstructure

Figure 2 shows the XRD patterns of SLMed Ti6Al4V alloy samples. Diffraction peaks corresponding to α Ti are detected in the as-deposited sample, with no obvious *β phase* peaks. Moreover, the α Ti diffraction peak for the as-deposited sample is slightly shifted to a higher angle relative to the standard position, indicating formation of an acicular *α' phase* [20]. This indicates that the as-deposited sample mainly consists of acicular *α' phase*, with a much smaller relative content of *β phase* and no obvious *β phase* diffraction peaks in the XRD patterns. After four different temperature heat treatments, the microstructure of SLMed Ti6Al4V alloy mainly consists of *α phase* and *β phase*. However, the relative content of *β phase* is still significantly smaller than that of *α phase*. As the heat treatment temperature increases from 800°C to 950°C, the diffraction peak intensity of the *α phase* of the sample gradually decreases, while that of the *β phase* continuously increases. This indicates that the relative content of *α phase* gradually decreases and the relative content of *β phase* gradually increases with the increasing heat treatment temperature.

Figure 3 shows the microstructure of SLMed Ti6Al4V alloy as-deposited sample. It can be seen that there are columnar crystals in the microstructure of the as-deposited sample. These irregularly arranged columnar crystals are incipient β grains that grow in the direction of the temperature gradient and through multiple deposition layers [21]. The irregular arrangement of the primary β grains is caused by the incomplete overlap of the melt pool of the previous layer with that of the next layer during the selective laser melting forming process [22]. These primary β grains are densely packed with fine acicular *α' phases* inside. This is due to the rapid cooling of the molten pool, which results in the formation of acicular *α' phase* as the incipient *β phase* has no time to transform to the *α phase*.
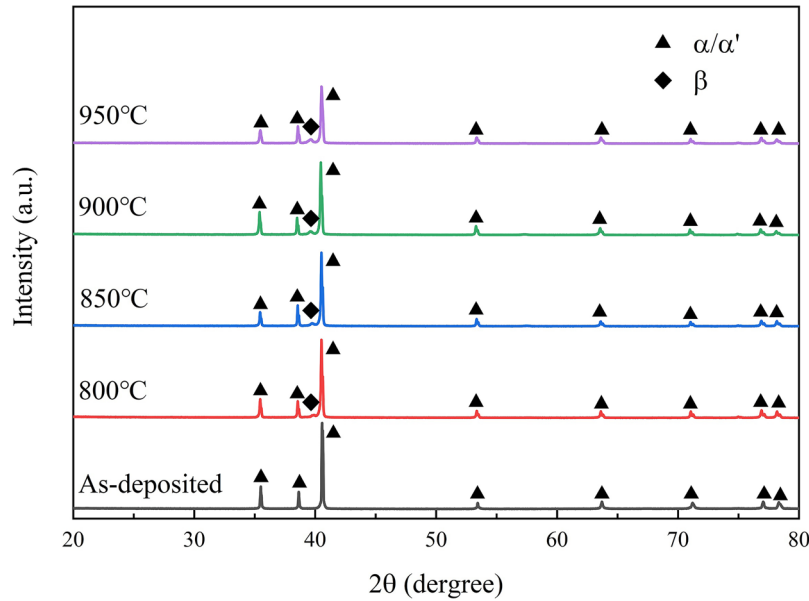
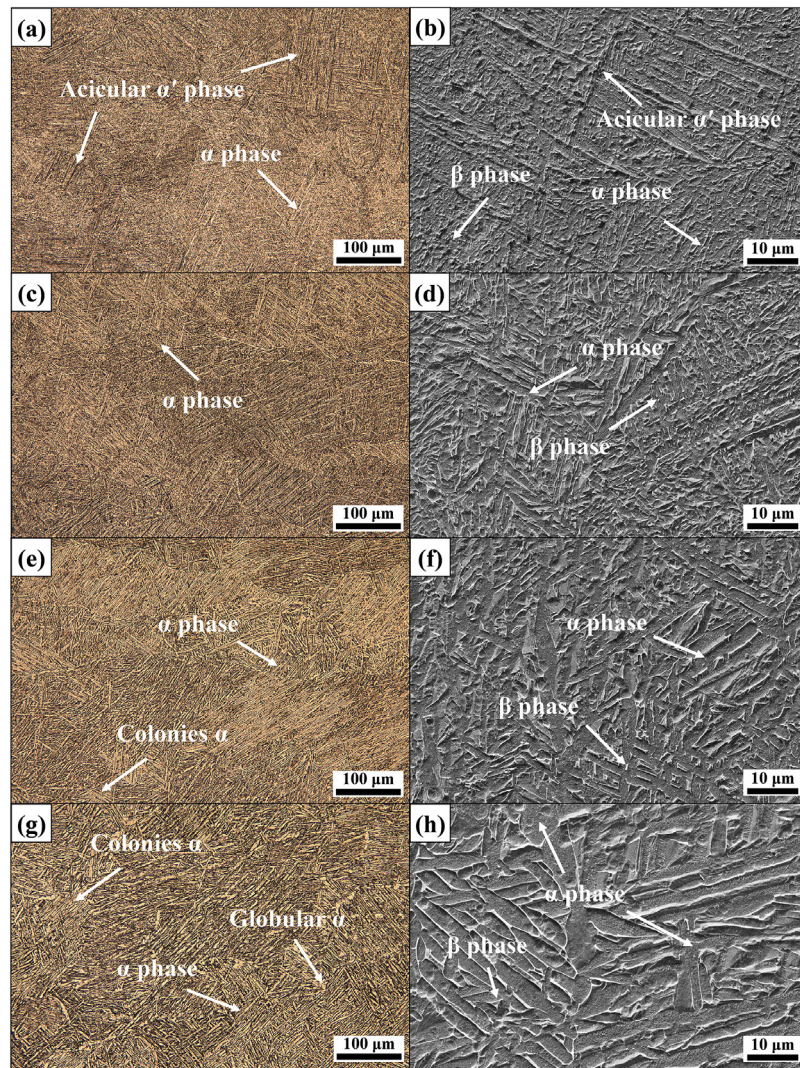**Figure 2:** XRD patterns of the SLMed Ti6Al4V alloy.
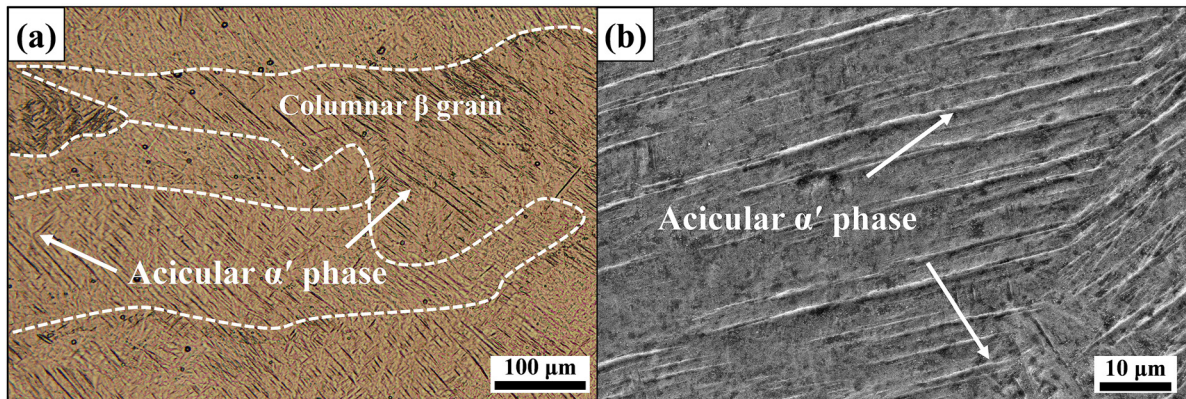
Figure 3: Microstructure of SLMed Ti6Al4V alloy as-deposited sample: (a) OM, (b) SEM.

Figure 4 shows the microstructure of the SLMed Ti6Al4V alloy after heat treatment. From Figure 4(a) and (b), acicular *α' phase* transformed to stable *α + β phase* under the high temperature condition of 800°C, forming a mixed microstructure of *α'* and *α + β phases* [23]. When the heat treatment temperature reaches 850°C, acicular *α' phase* disappear in the sample microstructure, replaced by a mesh basket organization consisting of *α + β phases* (as shown in Figure 4(c) and (d)). When the heat treatment temperature was 900°C, *α phase* in the sample microstructure coarsen, the mesh basket organization is destroyed with the appearance of colonies α, and the volume fraction of *β phase* increases. When the heat treatment temperature is increased to 950°C, *α phase* in the sample microstructure further coarsen and become platelet, and globular *α phase* appear, and the volume fraction of *β phase* further increases [24]. Combined with the above, it can be found that the acicular *α' phase* in the microstructure of SLMed Ti6Al4V alloy is gradually transformed into *α + β phases* with increasing heat treatment temperature, the volume fraction of *β phase* gradually increases, and *α phase* is gradually coarsened when the heat treatment temperature exceeds 850°C.
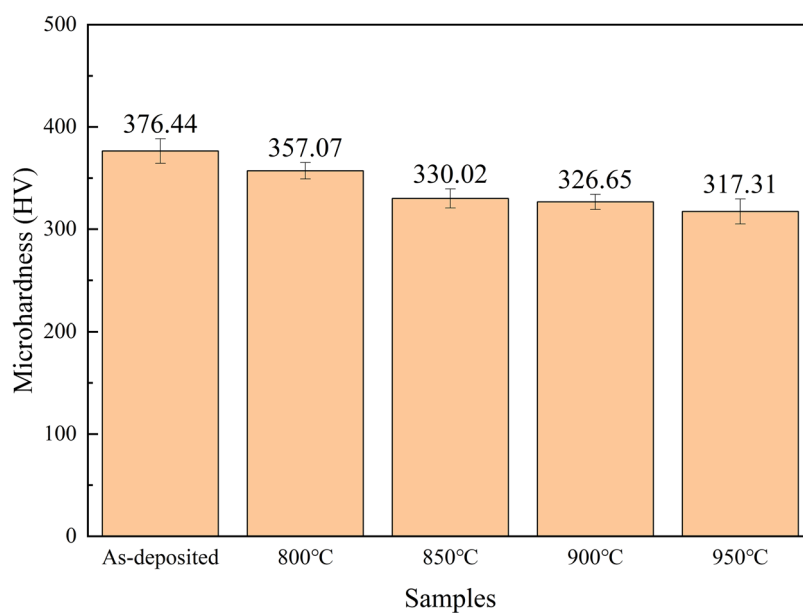
3.2. Mechanical properties

The microhardness of SLMed Ti6Al4V alloy is shown in Figure 5. From the figure, it can be seen that the microhardness of SLMed Ti6Al4V alloy decreased significantly after four heat treatments. The microhardness of SLMed Ti6Al4V alloy is mainly affected by the microstructure, and the microhardness of its microstructures is in the following order from largest to smallest: acicular *α' phase*, *α phase*, and *β phase* [23]. Combining the above microstructures, it can be found that there are a large number of acicular *α' phases* in the as-deposited sample, resulting in the highest microhardness of 376.44 HV. When the heat treatment temperature is 800°C, the
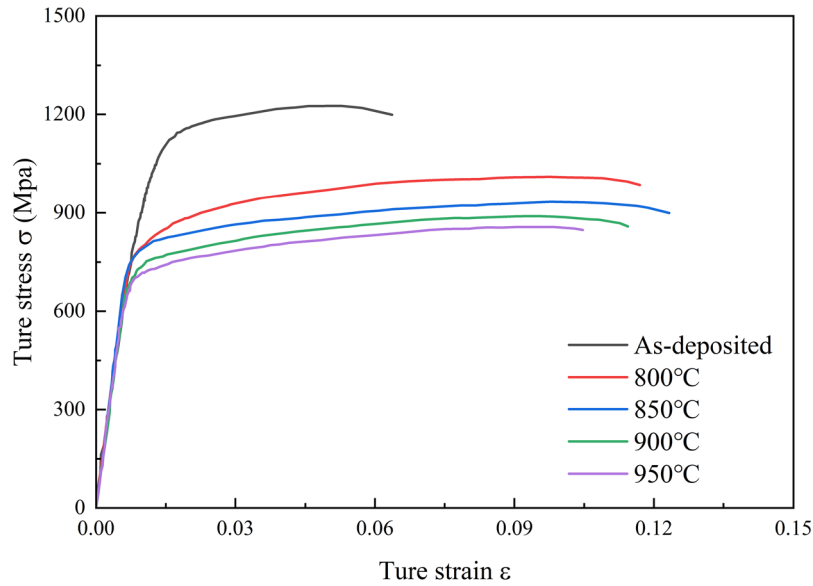
Figure 4: Microstructure of the SLMed Ti6Al4V alloy after heat treatment: (a) 800°C-OM, (b) 800°C-SEM, (c) 850°C-OM, (d) 850°C-SEM, (e) 900°C-OM, (f) 900°C-SEM, (g) 950°C-OM, and (h) 950°C-SEM.

Figure 5: Microhardness of the SLMed Ti6Al4V alloy.

Figure 6: Ture stress–strain curves of the SLMed Ti6Al4V alloy.

**Table 3:** Mechanical performance of the SLMed Ti6Al4V alloy.

MECHANICAL PROPERTIES	AS-DEPOSITED	800°C	850°C	900°C	950°C
Yield strength (MPa)	966.3	781.6	776.3	716.4	689.2
Tensile strength (MPa)	1171.5	933.8	868.3	825.1	790.9
The maximum principal stress (MPa)	1225.9	1009.8	933.7	889.8	856.7
Elongation (%)	6.6	12.4	13.6	12.2	11.1
(Tensile strength) × (Elongation) (GPa%)	7.7	11.6	11.8	10.1	8.8

microstructure of the sample is a mixture of acicular *α′ phase* and *α + β phases*, and therefore the microhardness is relatively high. And with the increase of heat treatment temperature from 850°C to 950°C, the acicular *α′ phase* has been completely decomposed, and the microstructure consists of *α + β phases*. And with the increase of temperature, the content of *α phase* gradually decreases, and the content of relatively soft *β phase* gradually increases, the grain grows and coarsens, so that the microhardness of the sample is reduced to 317.31HV.

Figure 6 shows the true stress-strain curves of SLMed Ti6Al4V alloy, with mechanical properties in Table 3. As heat treatment temperature increases, the strength and maximum principal stress of SLMed Ti6Al4V alloy gradually decreases, while elongation first increases then decreases. The tensile properties are influenced by microstructure, containing large acicular *α′ phases* in the as-deposited sample. This is characterized by high strength and low plasticity [25]. After heat treatment, the acicular *α′ phase* gradually transform into stable *α + β phases*, and the volume fraction of *β phase* increases compared to *α phase*. The *β phase* has lower strength but higher plasticity than the *α phase*. The as-deposited sample has the highest strength but the lowest elongation, with yield strength and tensile strength reaching 966.3 MPa and 1171.5 MPa, respectively, while elongation is only 6.6%. After heat treatment, the elongation of the samples increased significantly, with the sample heat-treated at 850°C achieving 13.6%, 106.1% higher than the as-deposited sample. However, the elongation decreased when the heat treatment temperature increased to 900°C. This is due to the disruption of the mesh basket organizational features in the microstructure of the sample and the formation of colonies of *α phase* that are prone to local stress concentration [26]. The elongation of the sample continued to decrease when the heat treatment temperature reached 950°C. This is due to further coarsening of the *α phase* in the sample into platelets and the appearance of globular α, resulting in large dislocation stresses and a decrease in elongation of the sample after heat treatment at 950°C to 11.1%.

To accurately evaluate comprehensive sample performance, we introduce the product of strength and elongation as a comprehensive mechanical property index. As shown in Table 3, the product of strength and elongation for SLMed Ti6Al4V alloy increases and then decreases with increasing heat treatment temperature.
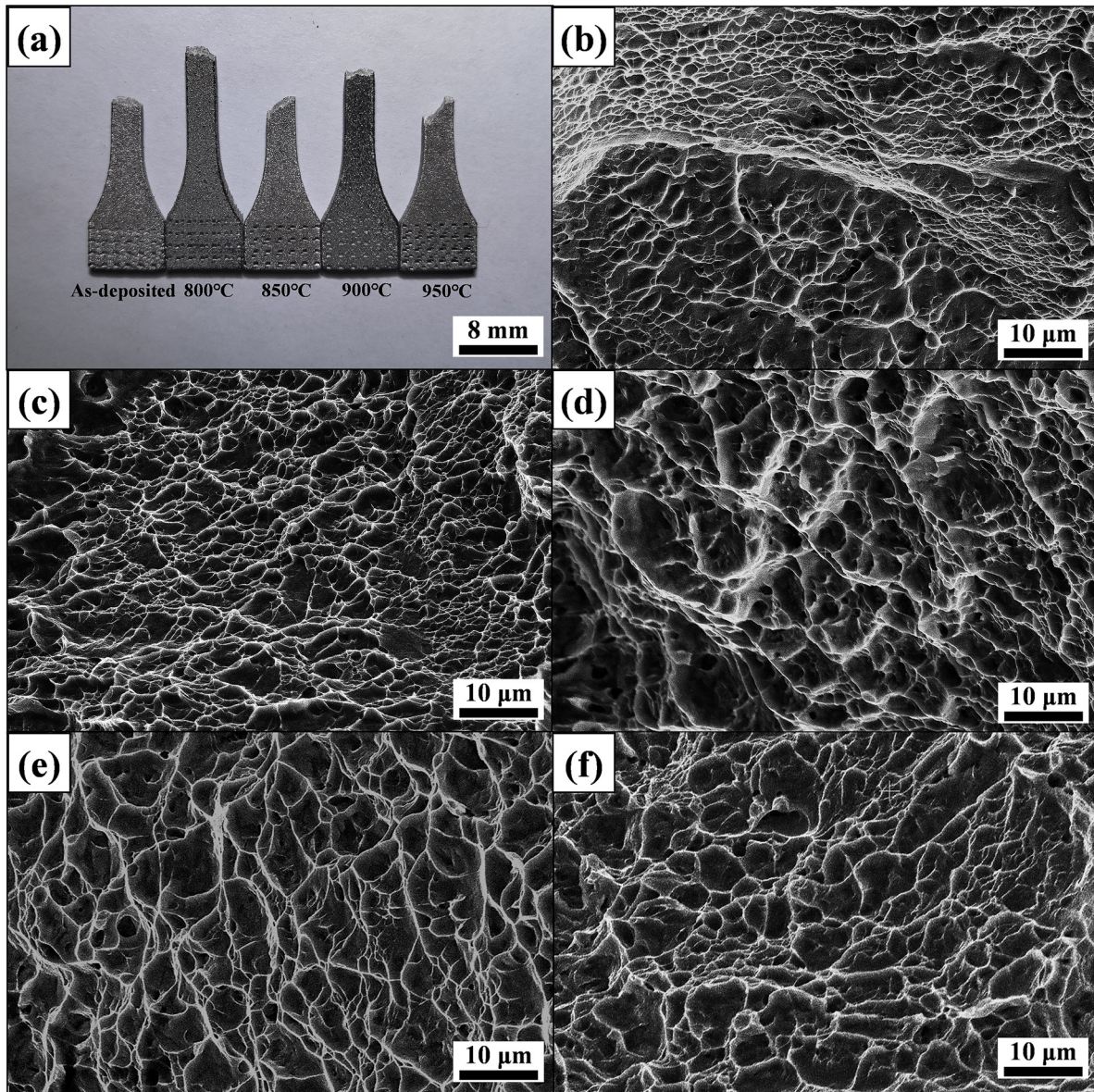
Figure 7: Tensile fracture morphology of the SLMed Ti6Al4V alloy: (a) Tensile fracture samples, (b) as-deposited, (c) 800°C, (d) 850°C, (e) 900°C, and (f) 950°C.

The sample exhibits optimal comprehensive mechanical properties at a heat treatment temperature of 850°C, with a product of strength and elongation reaching 11.8 GPa%.

Figure 7 shows the fracture morphology of tensile samples of SLMed Ti6Al4V alloy. All SLMed Ti6Al4V alloys exhibit ductile fracture at the macroscale (Figure 7(a)). Scanning electron microscope images (Figure 7(b–f)) show the tensile fracture of SLMed Ti6Al4V alloy. As-deposited sample (Figure 7(b)) exhibit numerous shallow, small ductile dimples around disintegration steps. This observation, combined with Figure 7(a), suggests mixed fracture dominated by ductile fracture. After heat treatment, ductile dimples on fracture surfaces deepened, enlarged, and became more dense, indicating all samples exhibited ductile fracture [27]. Samples heat-treated at 850°C exhibited the highest elongation, with larger, deeper, more dense dimples at fracture. These dimples formed due to gradual convergence of microscopic pores within the material during slip under tension, enhancing plasticity of heat-treated samples [28]. This result aligns with mechanical property test results discussed earlier.

3.3. Damage evolution

To study damage deformation of SLMed Ti6Al4V after different heat treatments, uniaxial tensile tests were performed using a material testing machine and laser range finder, with elastic modulus measured via
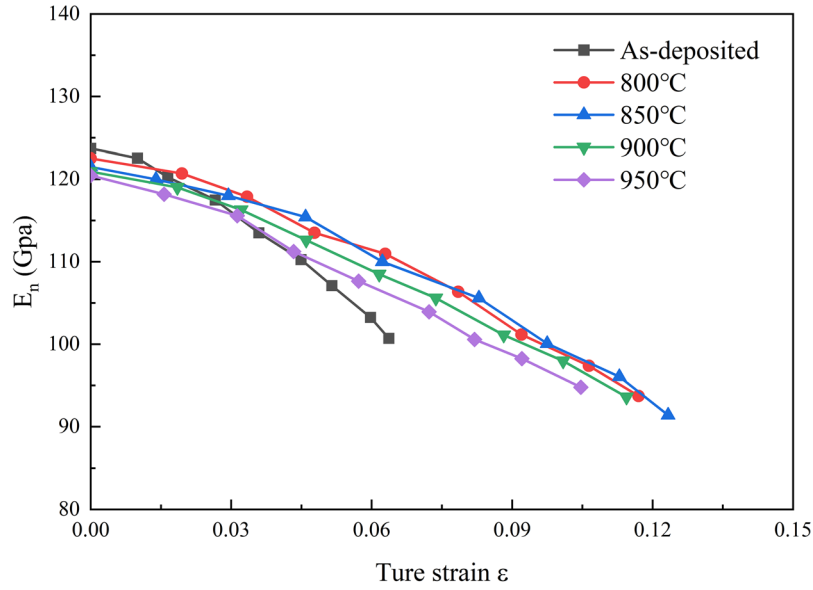
Figure 8: Variation of elastic modulus with macroscopic true strain for SLMed Ti6Al4V alloy measured by nanoindentation.
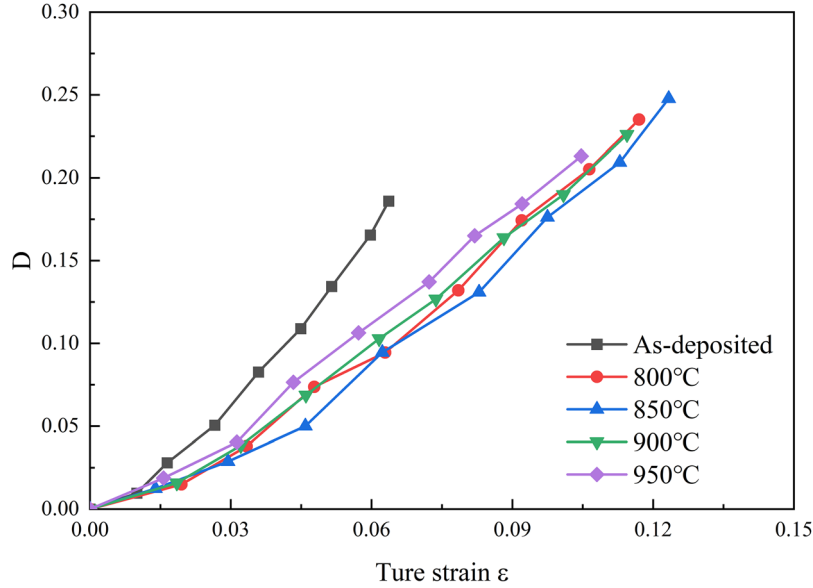
Figure 9: Evolution curves of damage factor *D* for the SLMed Ti6Al4V alloy.

nanoindentation at different strain stages. As shown in Figure 8, the modulus of elasticity of the sample decreases gradually with increasing true strain. The modulus of elasticity of the samples after heat treatment is slightly reduced compared to the as-deposited sample, and the modulus of elasticity decreases gradually with increasing heat treatment temperature.

As defined in the literature [29], the damage evolution of a material can be characterized by the modulus of elasticity, as shown in the following equation:

$$D = 1 - \frac{\tilde{E}_n}{E_{no}} \tag{1}$$

where *D* is the damage factor, E_{no} is the initial modulus of elasticity of the material, and $\tilde{E}_n$ is the actual modulus of elasticity of the material after being subjected to an applied load.

Figure 9 shows the evolution curve of damage factor *D* for SLMed Ti6Al4V alloy. As can be seen, with increasing true strain, *D* gradually increases and the damage degree of samples increases until failure. This is due to the material in tension, with increasing deformation, the elastic modulus gradually decreases, so the material's
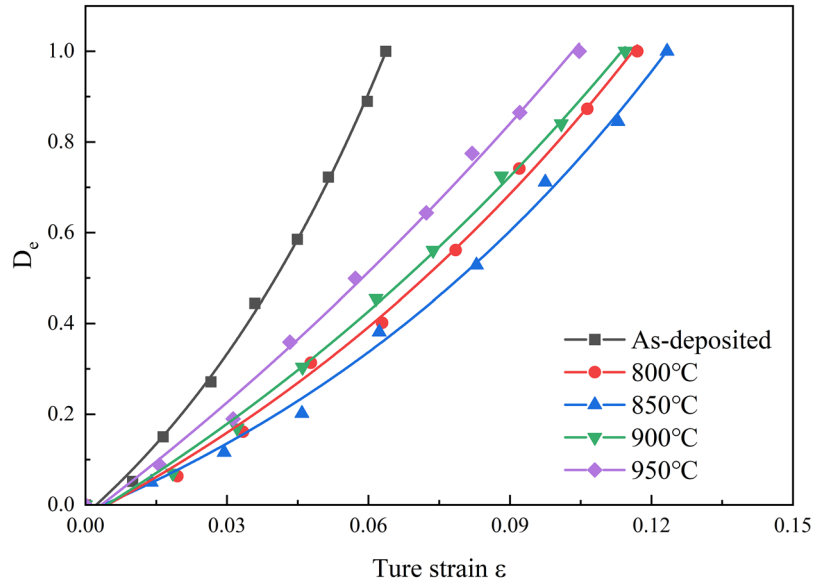
Figure 10: Evolution curves of normalization factor D_e for the SLMed Ti6Al4V alloy.

resistance to crack generation and propagation decreases, and damage increases. The as-deposited sample first enters the stage of rapid damage accumulation, and this stage in heat-treated samples lags significantly. With increasing heat treatment temperature, the rapid damage accumulation stage of samples lags; however, when the temperature increases to 900°C, this stage gradually advances.

To bring the research closer to the essence, achieve a change in damage from 0 to 1, and quantitatively characterize the degree of damage in the SLMed Ti6Al4V alloy, normalize formula (1) and define the normalization factor D_e as follows:

$$D_e = \frac{E_{no} - \tilde{E}_n}{E_{no} - E_{nf}} \qquad (2)$$

where D_e is the normalization factor and E_{nf} is the elastic modulus of the material at fracture failure.

The evolution curve of normalization factor D_e for SLMed Ti6Al4V alloy is plotted in Figure 10. From the figure, the evolution of D_e after different heat treatment temperatures resembles that of damage factor D both increase with true strain. The range of D_e is 0 to 1. When $D_e = 0$, the SLMed Ti6Al4V alloy is in its initial state with no damage; when $0 < D_e < 1$, the SLMed Ti6Al4V alloy is stretching and its degree of damage increases with D_e; when $D_e = 1$, the SLMed Ti6Al4V alloy is fractured. By fitting the D_e of the SLMed Ti6Al4V alloy with an exponential function, the damage evolution equations of the SLMed Ti6Al4V alloy are obtained as follow:

As-deposited sample:

$$D_e = 0.5704 e^{\frac{\varepsilon}{0.0621}} - 0.5916 \qquad (3)$$

800°C sample:

$$D_e = 0.7179 e^{\frac{\varepsilon}{0.1308}} - 0.7438 \qquad (4)$$

850°C sample:

$$D_e = 0.4733 e^{\frac{\varepsilon}{0.1075}} - 0.4901 \qquad (5)$$

900°C sample:

$$D_e = 1.0466 e^{\frac{\varepsilon}{0.1661}} - 0.1749 \qquad (6)$$

950°C sample:

$$D_e = 1.8254e^{\frac{\varepsilon}{0.2315}} - 1.8521 \tag{7}$$

The fitting equation is then combined to establish the general equation:

$$D_e = Ae^{\frac{-\varepsilon}{B}} + C \tag{8}$$

where A, B, C are material constants related to heat treatment temperature.

To distinguish the slow and rapid damage accumulation stages of SLMed Ti6Al4V alloy, this study defines a critical differentiation value D_{ec}, When $0 < D_e < D_{ec}$, the alloy is in the early deformation stage with slow damage accumulation; when $D_{ec} < D_e < 1$, the alloy enters rapid damage accumulation; and when $D_e = 1$, the alloy fractures. The Normalized Cockcroft & Latham damage model calculates D_{ec} for SLMed Ti6Al4V alloy [30].

$$D_{ec} = \int_0^{\varepsilon f} \left(\frac{\sigma_1}{\sigma_u} \right) d\varepsilon \tag{9}$$

where ε_f is the true strain at fracture; σ_1 is the maximum principal stress in tension; σ_u is the stress at the beginning of necking in tension (tensile strength); and ε is the true strain of the material.

Combined with Figure 10 and Table 3 through Equation (9), the ductility coefficient D_{ec} of the SLMed Ti6Al4V alloy can be obtained, and its corresponding true strain is the critical strain ε_c, as shown in Figure 11. As can be seen from the figure, both D_{ec} and ε_c increase first and then decrease with the heat treatment temperature. Among them, D_{ec} and ε_c of the sample with a heat treatment temperature of 850°C are the largest, and enter the rapid damage accumulation stage last.

3.4. Damage constitutive model

The constitutive model of a material is used to describe its mechanical properties, and damage under external loading affects these properties. Accurately describing the effect of damage in a constitutive model is an important aspect of constitutive model research. Therefore, this paper considers introducing a damage factor into the existing constitutive model to establish a damage constitutive model. The Ramberg-Osgood model is particularly suitable for metals hardened by plastic deformation, with smooth elastic-plastic transition. Based on true stress-strain curves of SLMed Ti6Al4V alloy before and after heat treatment (Figure 6), this paper adopts the Ramberg-Osgood model (Equation 10) as the initial model [31].

$$\varepsilon = \frac{\sigma}{E} + K \left(\frac{\sigma}{E} \right)^M \tag{10}$$
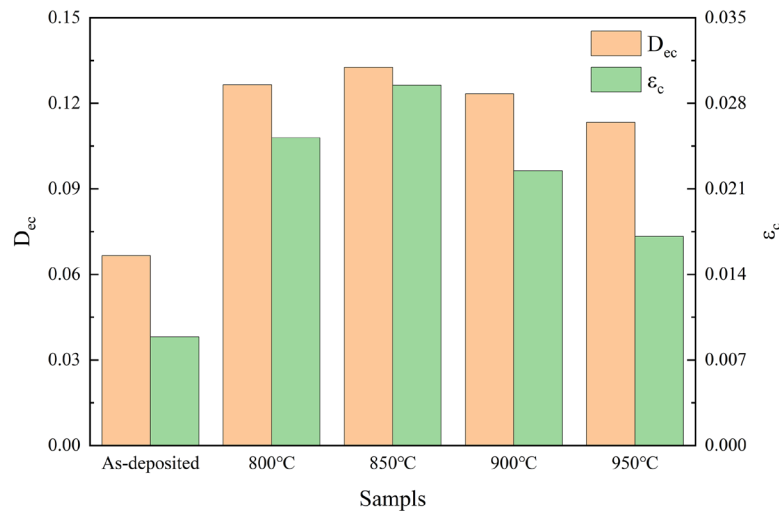
Figure 11: Critical damage factor D_{ec} and critical strain ε_c of the SLMed Ti6Al4V alloy.

where ε is the total strain, σ is the total stress, E is the modulus of elasticity, K is the strain hardening coefficient of the material, and M is the strain hardening index of the material.

Equation (10) can also be written in the following form:

$$\sigma = \begin{cases} E\varepsilon, \varepsilon \le \dfrac{\sigma_e}{E} \\ KE\varepsilon, \varepsilon > \dfrac{\sigma_e}{E} \end{cases} \tag{11}$$

where σ_e is the elastic limit of the material.

Based on the strain equivalence assumption proposed by Lemaitre, the effective stress is introduced into the deformation behavior of the damaged material, establishing the constitutive relationship between the undamaged and damaged materials. Substituting Equation 12 into Equation 11 establishes the damage constitutive model [32, 33]:

$$\tilde{\sigma} = \frac{\sigma}{(1-D)} \tag{12}$$
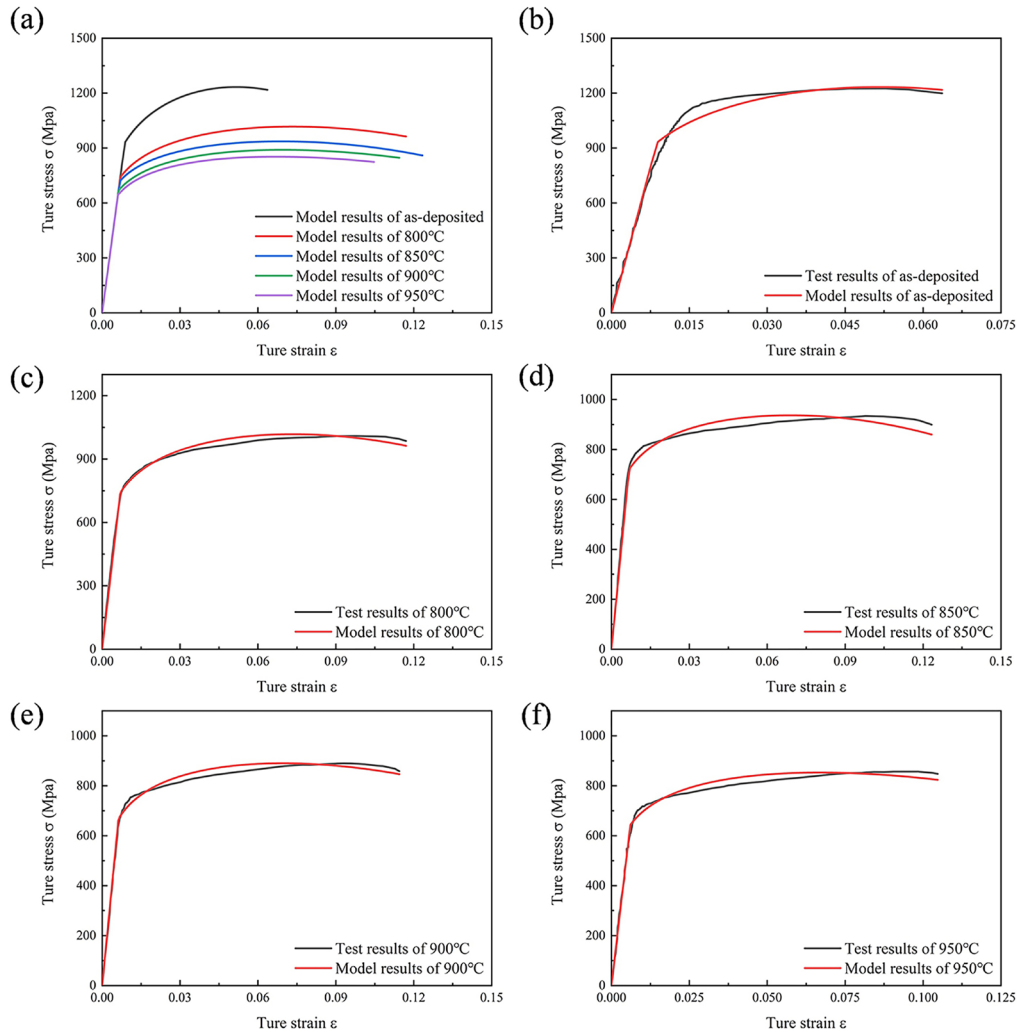
Figure 12: Damage constitutive model curves of SLMed Ti6Al4V alloy and results of comparison between damage constitutive model curves and experimental true stress-strain curves of SLMed Ti6Al4V alloy: (a) Damage constitutive model curves of SLMed Ti6Al4V alloy, (b) as-deposited, (c) 800°C, (d) 850°C, (e) 900°C, and (f) 950°C.

Table 4: Strain hardening coefficient *K* and strain hardening index *M* of the SLMed Ti6Al4V alloy.

SAMPLE	K	M
As-deposited	27.812	0.241
800°C	17.869	0.188
850°C	15.026	0.159
900°C	14.959	0.170
950°C	14.598	0.171

$$\sigma = \begin{cases} E\varepsilon, \varepsilon \leq \dfrac{\sigma_e}{E} \\ (1-D)KE\varepsilon, \varepsilon > \dfrac{\sigma_e}{E} \end{cases} \tag{13}$$

where σ is the true stress, $\tilde{\sigma}$ is the effective stress, ε is the true strain.

Calculation of the elastic stage of the true stress-strain curve in Figure 6, based on Hooke's law, confirms an elastic modulus of 106 GPa for the SLMed Ti6Al4V alloy. By fitting the true stress-strain curve according to Equation 13 (shown in Figure 12(a)), the parameters of the damage constitutive model for SLMed Ti6Al4V alloy can be obtained as shown in Table 4.

As shown in Figure 12(b~f), comparison of model curves derived from the established damage constitutive model with experimental true stress-strain curves shows that in the elastic deformation stage, the damage constitutive model for SLMed Ti6Al4V alloys before and after different heat treatments follows Hooke's law, with linear relationship between true stress and true strain. Model results agree well with test results. In the plastic deformation stage, the damage constitutive model results for SLMed Ti6Al4V alloys before and after different heat treatments correspond well with experimental results, with close agreement in trend and value. Comparison of modelled and experimental results shows that modelled results for SLMed Ti6Al4V alloys before and after different heat treatments fluctuate around experimental results with increasing true strain. The error between the model and test results for flow stress is within 7%, indicating the established damage constitutive model can accurately predict flow stress with plastic deformation of SLMed Ti6Al4V before and after different heat treatments. The damage constitutive model based on the damage factor can more realistically reflect the true stress-strain relationship of SLMed Ti6Al4V alloy, and the macroscopic true stress-strain relationship can be linked to the damage factor.

4. CONCLUSIONS

In this study, SLMed Ti6Al4V alloy with different heat treatment temperatures was used as the research object, and its influence on mechanical properties was analyzed by microstructure. The damage evolution law of SLMed Ti6Al4V alloy was quantitatively analyzed. The damage constitutive model of SLMed Ti6Al4V alloy with different heat treatment temperatures was also established, and the following conclusions were drawn:

(1) The acicular *α' phase* in the microstructure of the SLMed Ti6Al4V alloy gradually transforms into an *α + β phase* after heat treatment. With increasing heat treatment temperature, the *α phase* coarsens, the volume fraction of *β phase* increases. The microhardness, strength, and maximum principal stress of the SLMed Ti6Al4V alloy decreases from 376.44 HV, 1171.5 MPa and 1225.9 MPa to 317.31 HV, 790.9 MPa and 856.7 MPa. The elongation first increases from 6.6% to 13.6%and then decreases to 11.1%. As-deposited samples showed a mixed fracture pattern dominated by ductile fracture, and the fracture patterns of the heat-treated samples were all ductile fracture.

(2) The damage factor of SLMed Ti6Al4V alloy increases with increasing true strain. As-deposited samples first enter a rapid damage accumulation stage, with heat-treated samples exhibiting significantly lagged rapid damage accumulation. Higher heat treatment temperatures result in gradually lagged rapid damage accumulation of samples; however, at 900°C heat treatment, the rapid damage accumulation stage gradually advances. Damage is divided into slow and fast accumulation stages by a critical factor. The critical factor of SLMed Ti6Al4V alloy increases then decreases with increasing heat treatment temperature. Compared to other samples, the 850°C sample has the largest critical factor. A general equation for damage evolution of SLMed Ti6Al4V alloy at different heat treatment temperatures is established.

(3) Based on the theory of continuous damage mechanics, the Ramberg-Osgood model is introduced to establish the damage constitutive model of SLMed Ti6Al4V alloy under different heat treatment temperatures. The error between the model results of flow stress and the test results is within 7%. The model can reflect the true stress-strain relationship of SLMed Ti6Al4V alloy more realistically, and the macroscopic true stress-strain relationship can be linked to the damage factor.

5. ACKNOWLEDGMENTS

6. BIBLIOGRAPHY

[1] YING, L., ZHOUDE, Q., BENXIAN, W., "Research development and application of Ti6Al4V alloy", *Ordnance Material Science and Engineering*, v. 28, n. 1, pp. 47–50, Jan. 2005.

[2] HOTT, M.V.M., SILVA, L.A., SILVA, S.N., "Development of TiO_2 layer produced by electrochemical treatment on Ti6Al4V alloy: its physicochemical and mechanical characterization", *Matéria (Rio de Janeiro)*, v. 25, n. 4, pp. e–12902, Dec. 2020. doi: http://doi.org/10.1590/s1517-707620200004.1202.

[3] BAKER, T.N., "Titanium microalloyed steels", *Ironmaking & Steelmaking*, v. 46, n. 1, pp. 1–55, Jan. 2019. doi: http://doi.org/10.1080/03019233.2018.1446496.

[4] SUGAHARA, T., MONTORO, F.E., TAKAHASHI, R.J., *et al.*, "Microstructural characterization by EBSD of Ti-6Al-4V alloy with a SiC/Cr layer deposited by HiPIMS process before and after the creep tests", *Matéria (Rio de Janeiro)*, v. 27, n. 1, pp. e–13159, Apr. 2022. doi: http://doi.org/10.1590/s1517-707620220001.1359.

[5] JUNJIE, Z., YOUQIAG, W., CHENBING, N., *et al.*, "Research progress on microstructure and mechanical properties of titanium alloy by laser additive manufacturing", *Surface Technology*, v. 53, n. 1, pp. 15–32, Jun. 2024.

[6] LEI, L., XIAODONG, L., QIAO, L., *et al.*, "Effect of heat treatment on the microstructure and surface damage evolution of selective-laser-melted IN718 alloy", *Matéria (Rio de Janeiro)*, v. 29, n. 1, pp. e20230311, Feb. 2024. doi: http://doi.org/10.1590/1517-7076-rmat-2023-0311.

[7] GONZALEZ, Y.E., MENDOZA, J.M., DURÁN, J.R., *et al.*, "Effect of printing parameters on mechanical properties and processing time of additively manufactured parts", *Matéria (Rio de Janeiro)*, v. 28, n. 3, pp. e20230111, Jul. 2023. doi: http://doi.org/10.1590/1517-7076-rmat-2023-0111.

[8] LIU, S., SHIN, Y.C., "Additive manufacturing of Ti6Al4V alloy: a review", *Materials & Design*, v. 164, pp. 107552, Feb. 2019. doi: http://doi.org/10.1016/j.matdes.2018.107552.

[9] KARIMI, J., KOLLO, L., PRASHANTH, K.G., "Tailoring anisotropy and heterogeneity of selective laser melted Ti6Al4V alloys", *Transactions of the Indian National Academy of Engineering*, v. 8, n. 2, pp. 245–251, Feb. 2023. doi: http://doi.org/10.1007/s41403-023-00393-z.

[10] ZHEN, D., YUYUE, W., ANFENG, Z., *et al.*, "Effect of different heat treatments on microstructure, properties, and anisotropy of SLM TC4", *Chinese Journal of Lasers*, v. 48, n. 8, pp. 97–108, Apr. 2022.

[11] JABER, H., KÓNYA, J., KULCSÁR, K., *et al.*, "Effects of annealing and solution treatments on the microstructure and mechanical properties of Ti6Al4V manufactured by selective laser melting", *Materials (Basel)*, v. 15, n. 5, pp. 1978, Mar. 2022. doi: http://doi.org/10.3390/ma15051978. PubMed PMID: 35269207.

[12] JIANQIANG, G., WENQIANG, D., LU, Z., "Study on heat treatment of TC4 ALLOY FORmed by SLM PRINTING", *Applied Lase*, v. 40, n. 3, pp. 404–408, Jun. 2020.

[13] LIANG, Z., SUN, Z., ZHANG, W., *et al.*, "The effect of heat treatment on microstructure evolution and tensile properties of selective laser melted Ti6Al4V alloy", *Journal of Alloys and Compounds*, v. 782, pp. 1041–1048, Apr. 2019. doi: http://doi.org/10.1016/j.jallcom.2018.12.051.

[14] BO, C., FUGUO, L., MIN, H., "Experimental characterization of damage variables of ductile metal", *Rare Metal Materials and Engineering*, v. 40, n. 11, pp. 2022–2025, Nov. 2011.

[15] ALHARBI, K., GHADBEIGI, H., EFTHYMIADIS, P., *et al.*, "Damage in dual phase steel DP1000 investigated using digital image correlation and microstructure simulation", *Modelling and Simulation*

in Materials Science and Engineering, v. 23, n. 8, pp. 085005, Oct. 2015. http://doi.org/10.1088/0965-0393/23/8/085005.

[16] LEI, L., ZHIMING, S., LI, Z., "Microstructural evolution of H62 copper alloy and T2 pure copper in different plastic deformation under tensile landing", *Rare Metal Materials and Engineering*, v. 46, n. 12, pp. 3589–3594, Dec. 2017. doi: http://doi.org/10.1016/S1875-5372(18)30042-0.

[17] HAN, S., DINH, T.D., BAERE, D.I., *et al*., "Study of the effect of defects on fatigue life prediction of additive manufactured Ti-6Al-4V by combined use of micro-computed tomography and fracture-mechanics-based simulation", *International Journal of Fatigue*, v. 180, pp. 108110, Mar. 2024. doi: http://doi.org/10.1016/j.ijfatigue.2023.108110.

[18] LEI, Z., YANG, L., JINHUI, M., *et al*., "Dynamic mechanical properties and constitutive relationship of selective laser melted Ti-6Al-4V alloy", *Explosion and Shock Waves*, v. 42, n. 9, pp. 90–99, Dec. 2021.

[19] PENG, Z.S., JI, H.C., PEI, W.C., *et al*., "Constitutive relationship of TC4 titanium alloy based on back propagating (BP) neural network (NN)", *Metalurgija*, v. 60, n. 3–4, pp. 277–280, Jul. 2021.

[20] GU, D., HAGEDORN, Y.C., MEINERS, W., *et al*., "Densification behavior, microstructure evolution, and wear performance of selective laser melting processed commercially pure titanium", *Acta Materialia*, v. 60, n. 9, pp. 3849–3860, May. 2012. doi: http://doi.org/10.1016/j.actamat.2012.04.006.

[21] HE, B., WU, W., ZHANG, L., *et al*., "Microstructural characteristic and mechanical property of Ti6Al4V alloy fabricated by selective laser melting", *Vacuum*, v. 150, pp. 79–83, Apr. 2018. doi: http://doi.org/10.1016/j.vacuum.2018.01.026.

[22] KUMAR, P., PRAKASH, O., RAMAMURTY, U., "Micro-and meso-structures and their influence on mechanical properties of selectively laser melted Ti-6Al-4V", *Acta Materialia*, v. 154, pp. 246–260, Aug. 2018. doi: http://doi.org/10.1016/j.actamat.2018.05.044.

[23] LIU, X., CUI, W., WANG, Y., *et al*., "Effects of heat treatment on the microstructure evolution and mechanical properties of selective laser melted TC4 titanium alloy", *Metals*, v. 12, n. 5, pp. 702, Apr. 2022. doi: http://doi.org/10.3390/met12050702.

[24] ÖNDER, S., SAKLAKOĞLU, N., SEVER, A., "Selective laser melting of Ti6Al4V alloy: effect of post-processing on fatigue life, residual stress, microstructure, microhardness and surface roughness", *Materials Characterization*, v. 196, pp. 112571, Feb. 2023. doi: http://doi.org/10.1016/j.matchar.2022.112571.

[25] YUHAI, L., BAIQIANG, Z., YUSHENG, C., *et al*., "Effect of low and high double heat treatment on fracture toughness of tc4 titanium alloy fabricated by selective laser melting", *Rare Metal Materials and Engineering*, v. 51, n. 5, pp. 1864–1872, May. 2022.

[26] LI, C., DENFAN, W., ZEQING, Y., *et al*., "Effect of heat treatment on microstructure and properties of TC4 alloys fabricated by selective laser melting", *Journal of Beijing University of Technology*, v. 49, n. 9, pp. 970–979, Jul. 2023.

[27] YANG, X., LI, Y., DUAN, M., *et al*., "An investigation of ductile fracture behavior of Ti6Al4V alloy fabricated by selective laser melting", *Journal of Alloys and Compounds*, v. 890, pp. 161926, Jan. 2022. doi: http://doi.org/10.1016/j.jallcom.2021.161926.

[28] DING, H., ZHANG, J., LIU, J., *et al*., "Effect of volume energy density on microstructure and mechanical properties of TC4 alloy by selective laser melting", *Journal of Alloys and Compounds*, v. 968, pp. 171769, Dec. 2023. doi: http://doi.org/10.1016/j.jallcom.2023.171769.

[29] LEMAITRE, J., DUFAILLY, J., "Damage measurements", *Journal of Alloys and Compounds*, v. 28, n. 5–6, pp. 643–661, 1987.

[30] JINGLI, Z., JINPING, W., YUANYAN, L., *et al*., "Determination of critical damage values of Ti600 alloy based on Normalized Cockcroft & Latham ductile damage criterion", *Journal of Materials Engineering*, v. 47, n. 7, pp. 121–125, Jul. 2019.

[31] ARRAYAGO, I., REAL, E., GARDNER, L., "Description of stress-strain curves for stainless steel alloys", *Materials & Design*, v. 87, pp. 540–552, Dec. 2015. doi: http://doi.org/10.1016/j.matdes.2015.08.001.

[32] ZHIQIAN, R., ZONGYUE, Y., XUN, C., "Study on wire rope elastic-plastic damage constitutive model", *Jixie Gongcheng Xuebao*, v. 53, n. 1, pp. 121–129, Jan. 2021.

[33] ZHANG, Z., XU, Y., QIN, G., *et al*., "Deterioration of mechanical properties and the damage constitutive model of corroded steel in an industrial environment", *Materials (Basel)*, v. 15, n. 24, pp. 8841, Dec. 2022. doi: http://doi.org/10.3390/ma15248841. PubMed PMID: 36556647.